Thermal Science and Engineering Progress 47 (2024) 102298

Contents lists available at ScienceDirect

Thermal Science and Engineering Progress

journal homepage: www.sciencedirect.com/journal/thermal-science-and-engineering-progress

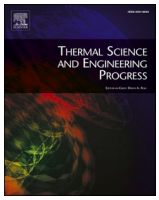

Advanced Phase-Change Intermediate Heat Exchanger Development for Multistage Thermoelectric Heat Pumps

I. Erro, P. Aranguren *, P. Alegría, A. Rodriguez, D. Astrain

Institute of Smart Cities, Public University of Navarre, Pamplona, Spain

ARTICLE INFO

Keywords:
Thermoelectric heat pump
Multistage
Heat exchanger
thermal resistance, COP enhancement

ABSTRACT

The need to reach a full energy decarbonisation is well known. Heating and cooling consumption is almost half of the global energy end-use. Thus, development of low-carbon and highly efficient power-to-heat technologies must be developed. In this work, the use of thermoelectric technology working as a heat pump is proposed to heat up an airflow of 38 m^3/h. Two different prototypes of multistage thermoelectric heat pumps have been developed and compared based on monophasic and phase-change intermediate heat exchangers. The reduced thermal resistance obtained for the novel phase-change heat exchanger increases the heat flux supplied to the airflow and reduces the consumed power of the system, outperforming the operation of the monophasic thermoelectric heat pump between a 30 and a 67 %. The novel multistage phase-change heat pump obtains experimental COP values between 3.25 and 1.26 when the airflow rises its temperature from 3.5 °C to 23.5 °C. Additionally, this experimental study proves a new methodology to calculate the supplied heat flux to the airflow. The validation of this technology proves a discrepancy of ± 9 % when this novel technology is compared to the conventional one based on the airflow temperature rise.

1. Introduction

The need to diminish greenhouse gas emissions in order to stop the climate change is generally known. As the International Renewable Energy Agency (IRENA) reveals, the energy system electrification is a top priority in the short and medium term to reach a full decarbonisation and to keep the rise in global temperatures below 2 °C [1]. In addition, the current geopolitical situation due to the invasion of Ukraine has increased the necessity to reduce the dependence on fossil fuels. In this line, electrification of the energy system must be combined with high penetration of renewable energies into the energy mix [2]. For this reason, European Union countries have set ambitious targets in line with the 2050 objectives in pursuit of a 100 % renewable future [3]. Thus, clean electricity becomes the principal fuel in the current energy transition. Energy demand is classified in four principal final uses: residential, commercial, industrial and transportation. In 2021, heat and cooling consumption accounted for almost 50 % of the global energy end-use, where the share of natural gas in the heating mix was over 40 % in the European Union and more than 60 % in the United States [4]. Therefore, the development of low-carbon and high-efficient electric Power-to-Heat (PtH) technologies has become necessary.

The most straightforward PtH devices are the electrical resistance heaters. The conversion of electrical power into heat energy is driven by Joule effect due to the current flow through a resistor. This PtH process achieves an efficiency of 100 %, transforming all consumed electricity into heat energy [5]. The major advantages of this technology are its scalability and ease of control. They are generally used for heating demand in residential and the industrial sector as electric boilers or electric heaters for water and space heating [6], which typically are provided as storage heaters or convection heaters, respectively [7]. Electrical resistance heaters are often used in industrial and agricultural procedures where the temperature control has high importance [8,9].

A promising PtH technology is the use of heat pumps for heating. In 2021 the use of heat pumps (HPs) reached to 190 million units for heating [4]. Moreover, in the Net Zero Emissions by 2050 Scenario, the installed HPs are pretended to reach 600 million units by 2030 [10]. The interest augmentation on heat pumps arises from their capacity of achieving better heating performance than electrical heaters, as the heat dissipated by a heat pump is the sum of the heat absorbed from the cold reservoir and the electrical power consumption. Up until now, the most used HP technology is the vapour compression heat pump (VCHP) that is based on a cycle that incorporates many components as an evaporator, a compressor, a condenser, and an expansion device, along with security

* Corresponding author.
E-mail address: patricia.arangureng@unavarra.es (P. Aranguren).

https://doi.org/10.1016/j.tsep.2023.102298
Received 17 August 2023; Received in revised form 26 October 2023; Accepted 18 November 2023
Available online 23 November 2023

Nomenclature

A	Airflow duct area, m^2
a	Equivalent contact radius ($\sqrt{(Am/\pi)}$), m
A_e	Monophasic intHX heat transfer area, m^2
A_m	TEM area/contact area, m^2
b	Equivalent plate radius ($\sqrt{(Ae/\pi)}$), m
B_i	Biot number
b_R^2	Systematic standard uncertainty
COP	Coefficient of performance
c_p	Heating capacity, J/kgK
$\Delta T_{sources}$	Temperature differences between sources, °C
I	Current supply, A
k	Thermal conductivity, W/mK
L	Monophasic intHX length, m
$\dot{m}_a$	Mass airflow (ρAv), kg/s
$\dot{Q}$	Heat flow, W
$\dot{Q}_{c,i}$	Absorbed heat flow by i MTEHP, W
$\dot{Q}_{h,i}$	Generated heat flow by i MTEHP, W
R	Thermal resistance, K/W
R_{cHX}	Cold side HX thermal resistance, K/W
R_{cond}	Conduction thermal resistance, K/W
R_{hHX}	Hot side HX thermal resistance, K/W
R_{intHX}	Intermediate HX thermal resistance, K/W
R_{spread}	Spreading thermal resistance, K/W
$S_{\bar{R}}^2$	Random standard uncertainty
t	Monophasic intHX thickness, m
T	Temperature, °C
T_{air}	Airflow temperature ($(T_{in,i} + T_{out,i})/2$), °C
T_{amb}	Ambient temperature, °C
$T_{c,i}^j$	Cold temperature of j stage of i MTEHP, °C
T_{cold}	Cold temperature of a HX, °C
$T_{h,i}^j$	Hot temperature of j stage of i MTEHP, °C
T_{hot}	Hot temperature of a HX, °C
$T_{in,i}$	Inlet temperature of i MTEHP, °C
T_{insu}	Insulation temperature, °C
$T_{out,i}$	Outlet temperature of i MTEHP, °C
U_R	Expanded uncertainty at 95 % level of confidence
V	Voltage supply, V
v	Airflow velocity, m/s
w	Monophasic intHX width, m
$\dot{W}_{e,i}$	TEMs power consumption of i MTEHP, W

Acronyms

cHX	Cold side heat exchanger
GWP	Global warming potential
HX	Heat exchanger
HP	Heat pump
hHX	Hot side heat exchanger
intHX	Intermediate heat exchanger
MTEHP	Multistage Thermoelectric Heat Pump
PtH	Power to heat
TES	Thermal energy storage
TEHP	Thermoelectric heat pump
TEM	Thermoelectric module
VCHP	Vapour compression heat pumps

Greek Symbols

ε	Dimensionless contact radius (a/b)
λc	Empirical parameter given by Eq(4)
ρ	Density, kg/m^3
τ	Dimensionless plate thickness(t/b)
Ψ	Dimensionless Constriction resistance

elements. However, an alternative to VCHP is the use of thermoelectric modules (TEMs) working as a heat pump. When a current is supplied, the TEM pumps the heat from the cold reservoir to the hot reservoir by the Peltier effect [11], performing as a thermoelectric heat pump (TEHP). This technology presents many advantages such as compactness, noiseless, no refrigerants, scalability, easy and accurate temperature control, reliability, and no moving parts. Additionally, thermoelectric heat pumps are often used in dehumidifiers [12], water heaters [13], clothes dryers [14], water generators [15] and other applications.

In recent years there has been an increase in the interest in the use of TEHPs in heating and air conditioning for buildings [16–19]. Lim et al. [16] optimized the arrangement and spacing of TEMs to obtain uniform temperature distribution on the surface of a thermoelectric radiant cooling panel for air-conditioning. Kim et al. [17] studied the use of TEHP for heating energy-efficient buildings, where they optimized the number of TEHP and current supply for three different cases: air-to-air heat exchanger, earth-to-air heat exchanger and no additional heat exchanger. Diaz de Garayo et al. [18] proposed a heating and cooling ventilation air conditioning system based on the combination of an air-to-air TEHP with phase-change heat exchangers. Hou et al. [19] studied the performance of a thermoelectric heat pump with recirculation and regenerative heat recovery. All those studies demonstrates the potential of the use of thermoelectric technology in buildings air-conditioning. Nevertheless, it can be noted how the temperature difference between reservoirs affects directly the TEHP performance. The higher the temperature difference between the hot and cold reservoirs, the lower COP of a TEHP becomes [17–20]. For this reason, it is necessary to study advanced TEHP configurations to enable a better performance when high temperature differences are necessary, extending the thermoelectric heat pump working range to other scenarios.

Thus, the interest in multistage thermoelectric heat pump (MTEHP) configurations shows up, which have been largely studied from a computational point of view for heat pumps in cooling applications [21–24]. All these studies present the dependency of MTEHP on multiple variables, such as: electric connection of stages, total applied voltage; voltage ratio between stages; inter-stage thermal resistance; and thermocouple properties such as number, area, length, ratio of thermocouples between stages and distribution. Wang et al. [21] stated that a ratio of the number of thermocouples between stages among 1.73–2.33 achieves maximum COP values and maximum temperature differences when a uniform temperature distribution between stages is conducted. Sun et al. [22] demonstrated that a parallel-connected MTEHP with a ratio of the number of thermocouples of 2 and optimized voltage ratio exhibits a power consumption reduction of approximately 50 % when compared to the series configuration. Chen et al. [23] analysed the effect of the intermediate ceramic layer thickness between stages on COP values demonstrating that the reduction of the inter-stage thermal resistance improves the overall performance. Cheng et al. [24] optimized the applied electrical current and the number of thermocouples of each stage, taking into account the effect of contact and spreading thermal resistance between stages.

Regarding TEHP for heating applications, the research on MTEHP is scarce, and it has only been conducted by computational means. Chen et al. [25] demonstrated that exists an optimal ratio of number of thermocouples between stages. Nami et al. [26] computationally demonstrated that using a thermoelectric heat pump with more than one stage results in better performance than a simple system for heating,

being able to operate at higher temperature differences with higher COP values. Chen et al. [27] optimized a two-stage TEHP connected to a two-stage thermoelectric generator where the influence of different temperature heat sinks on the optimal current, heating capacity and COP have been studied. Arora et al. [28] stated that a parallel connection of an optimized MTEHP, compared to series connection between stages, obtains higher COP values for heating. Nevertheless, none of these researches focus on the study of the thermal behaviour of the heat intermediate HXs (intHXs) and its influence on the operation of the whole TEHP for heating applications. The computational studies include negligible influence of the intermediate HXs [25–28] when it is known that this thermal resistance affects the operation of MTEHP [23,24].

In this work the influence of the intHX on MTEHPs intended to efficiently heat up an airflow has been experimentally evaluated. To that purpose, two different multistage TEHPs using different intermediate HX between stages have been designed and experimentally tested for the first time. A phase-change intHX has been developed to quantify the operation improvement of a MTEHP when compared to a MTEHP equipped with a conventional intHX. To that purpose, firstly, the two different intHX have been designed, developed and thermally characterized. Then, the two MTEHP full prototypes, each one including each type of intHX, have been built and tested in order to quantify the operation improvement when optimising the intHX. In addition, a novel method for calculating the COP based on the energy balance of a TEHP is proposed and validated with experimental results.

2. Components description

The literature shows different studies of multistage thermoelectric heat pump for different applications. However, no one has studied the influence of using different intermediate heat exchangers in a multistage configuration for a heating applications. In the present study, two MTEHP prototypes are built to experimentally study their performance and quantify the influence of the intHX on their *COP*. The prototypes are based on commercial modules from Marlow, RC12-6-01LS. Each module is composed of 127 thermocouples with a cross section area of 1.4 x 1.4 mm^2, a length of 1.15 mm, and external dimension of 40 x 40 mm^2 [29]. Each MTEHP has been designed with a two-stage configuration and a ratio of number of thermocouples between stages of two, one module in the first stage and two in the second one, following the optimum values that could be encountered in the literature [26].

The heat exchangers included into a TEHP play a crucial role on the operation of the system. Indeed, it has been demonstrated how the use of HX with a low thermal resistance (R) substantially improves the performance of the thermoelectric systems [30]. Each developed MTEHP prototype presents three HXs: the hot-side heat exchanger (hHX), the intermediate heat exchanger and the cold side heat exchanger (cHX), as shown in Fig. 1.

For the hHX the commercial, CR-1400 ARGB (Jonsbo) phase-change HX has been used to dissipate the generated heat. This heat exchanger includes 4 " U shape" copper heat pipe tubes with an external diameter of 6 mm and a total length of 300 mm. Additionally, 41 aluminium fins are included to improve heat dissipation. In contrast, a finned dissipater has been fabricated to use it as the cHX for absorbing the heat from the ambient. It is based on an aluminium finned block with a base of 73 x 73 mm^2 and 14.5 mm of height, with 15 fins which height, spacing and thickness are: 38.5; 3.4 and 1.6 mm, respectively. In addition, a 1.5 thick groove has been made in the cHX base to introduce a sensor to measure the temperature of the cold side ($T^1_{c,i}$) of the thermoelectric module. Additionally, an axial flow fan was located facing the fins in order to control the ambient airflow. Regarding the intHX, two different intermediate heat exchangers have been developed, each one based on a different heat transfer mechanism in order to measure their influence on the performance of the system.

2.1. Monophasic intHX

The monophasic intHX is based on heat transfer by conduction phenomena through a solid-state material. In this case, an aluminium block has been used. The design should have the lowest total thermal resistance (R), which is calculated by Eq.(1).

$$R = R_{cond} + R_{spread} \tag{1}$$

The conduction thermal resistance (R_{cond}) is calculated by Eq. (2), which represents the resistance of the object to the heat flow, where t stands for thickness of the aluminium block, k is the thermal conductivity and A_e represents the heat transfer area.

$$R_{cond} = \frac{t}{kA_e} \tag{2}$$

However, when heat is transferred through a solid material the spreading phenomenon appears when the heat source does not match the heat transfer area. The spreading thermal resistance (R_{spread}) occurs when the heat flows out of a narrow region into a larger cross-sectional area. In this prototype, the heat from the 1st stage TEM needs to be spread into a higher area, the 2nd stage TEMs and therefore the spreading phenomena appears. The R_{spread} can be calculated by Eq. (3) [31], where Ψ is the dimensionless spreading resistance, calculated

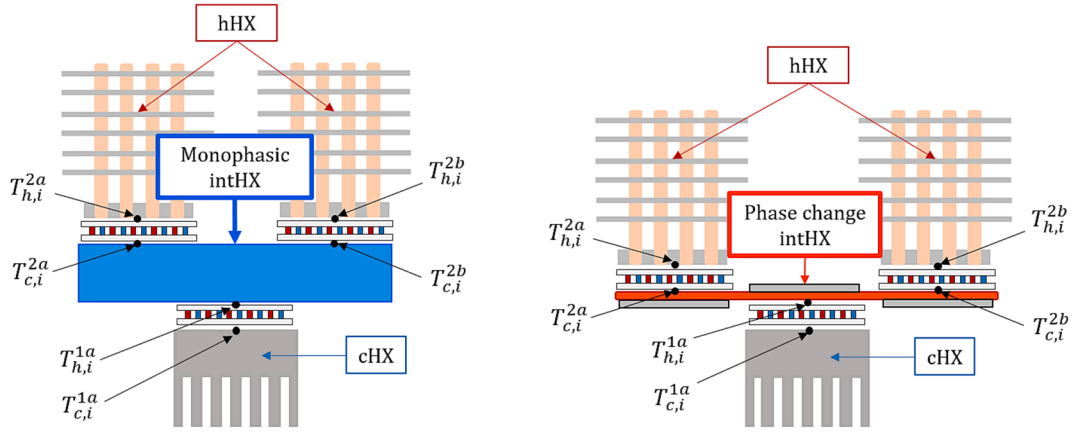

Fig. 1. Designed multistage TEHP with different intHX: a) monophasic intHX and b) phase-change intHX.

according to Eq.(4). A_m is the area of a thermoelectric module, Bi represents Biot number, λ_c is an empirical parameter given by Eq. (5), τ is the dimensionless monophasic heat exchanger thickness and ε is the dimensionless contact radius. This expression is valid for a ε range from 0.05 to 0.833 with Biot numbers higher than zero [31]. Therefore, depending on the dimensions, R_{spread} may present higher values than the conduction thermal resistance.

$$R_{spread} = \frac{\Psi}{k\sqrt{A_m}} \tag{3}$$

$$\Psi = \frac{1}{2}(1-\varepsilon)^{3/2}\frac{tanh(\lambda_c\tau)+\frac{\lambda_c}{Bi}}{1+\frac{\lambda_c}{Bi}\bullet tanh(\lambda_c\tau)} \tag{4}$$

$$\lambda_c = \pi + \frac{1}{\sqrt{\pi\varepsilon}} \tag{5}$$

Looking to the previous expressions, a thick block would help the spreading resistance, however, this would increase the conductive thermal resistance. Thus, an optimum value is needed to develop the most efficient intHX. A steady state thermal computational study using a CFD software was carried out in order to get the lowest R value for the monophasic intHX. The monophasic intHX is made out of aluminium and presents a rectangular geometry, with a length (L) of 150 mm and a width (w) of 40 mm, due to assembly restrictions. This study optimises the thickness (t) of the monophasic intHX (the distance between the 1st stage TEM and 2nd stage TEMs) to reach the minimum thermal resistance. The study considers an entering area for the heat flow from the 1st stage TEM, and two dissipation areas, 2nd stage TEMs, of 40 x 40 mm^2, as Fig. 2 a) shows. Heat flows of 50, 75 and 100 W have been analysed. Fig. 2 a) presents the temperature contour of the simulations and Fig. 2 b), presents the results where the minimum value of thermal resistance is 0.13 K/W with a thickness of 33 mm.

2.2. Phase-change intHX

A novel intHX based on liquid–gas phase-change has been developed in order to thermally connect the different stages in the developed MTEHP. The main advantage of using a phase-change heat exchanger is its capacity to spread the heat uniformly, aspect which is very beneficial for the thermal resistance of the system [30]. The proposed prototype uses heat pipes, where a phase-change cycle of the water happens. The heat load that emits the 1st stage provokes evaporation of the water that is near the TEM, the vapour travels to the ends of the heat pipes, where the TEMs of the 2nd stage absorb the heat, making the water to condensate, as Fig. 3 shows.

For this application, the designed intHX needs to be compact, robust, lightweight, ensure a good contact with the TEMs and it should be able to efficiently transfer the heat. Therefore, a custom made phase-change intHX has been built from 4 commercial heat pipes of 8 mm in diameter and 200 mm of length, ATS-HP5D5L20S77W-148 [32]. The tubes have been embedded in three different aluminium supports and the contact areas with the TEMs have been polished to improve the contact between the tubes and the modules, as it is shown in Fig. 4. The heat pipe tubes are in direct contact with the TEMs to ensure a minimum contact thermal resistance as well as the embedding process has been carefully performed to ensure the best thermal resistance.

3. Thermal characterization of the heat exchangers

An accurate methodology has been used in order to thermally characterize the different heat exchangers used in both prototypes [33]. The thermal resistance of the heat exchangers is obtained using Eq. (6), which relates the temperature difference between the hot (T_{hot}) and cold (T_{cold}) side of the HX that transfers the heat flow ($\dot{Q}$). A heating plate with a heat transfer area of 40 x 40 mm^2 has been used to control the heat flow through the HXs. By measuring its input voltage (V) and current (I) the heat flow is obtained using Eq.(7). Additionally, Table 1 presents the description of the measuring elements used, including their resolution and accuracy.

$$R = \frac{(T_{hot}-T_{cold})}{\dot{Q}} \tag{6}$$

$$\dot{Q} = V \bullet I \tag{7}$$

The thermal characterization tests for the different heat exchangers has been carried out inside a climate chamber at 26 °C. Fig. 5 shows the different assemblies used for each heat exchanger, as well as the location of the measurement proves used to calculate their thermal resistance. Table 2 includes the developed tests for each heat exchanger, where the heat flow ($\dot{Q}$) and airflow rate (vA) values were variated. The heat flow values are different for each heat exchanger, following their final operation at the MTEHP. For the hHX and cHX the airflow rate has been determined by measuring the velocity of the air in the duct at eleven horizontal equidistant positions to assess the speed profile. The measured point is separated 50 cm from the inlet to make sure the speed profile is fully developed, using an anemometer which precision and accuracy are listed in Table 1 [20]. Additionally, all the test benches have been properly insulated with rock wool to ensure no heat losses to the ambient. The latter fact is controlled by the temperature measurement of the insulation (T_{insu}), which for all the test the temperature difference between the ambient and the external side of the insulation was negligible, being less than 1 °C. All tests have been carried out for at least 15 min under stationary conditions with a sampling frequency of 30 s. Besides, each test was replicated three times in order to reduce the uncertainty of the measurements.

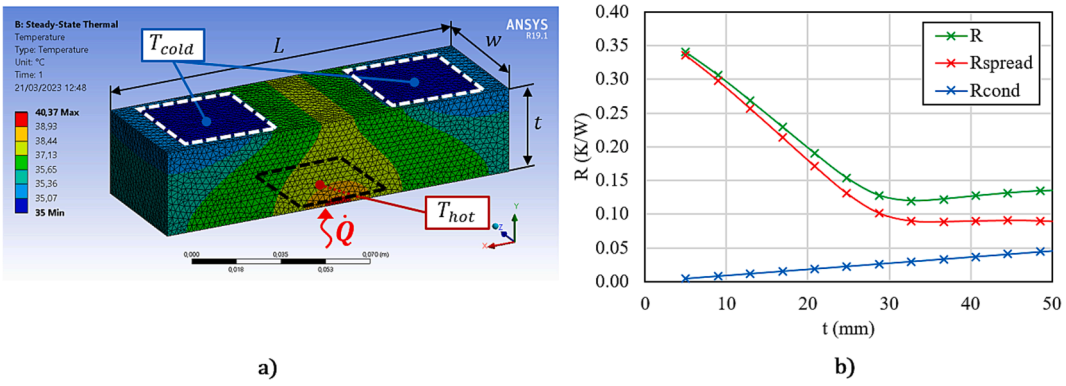

a) b)

Fig. 2. Steady state thermal study for thickness optimization a) Temperature distribution b) Total, spreading and conduction thermal resistance as a function of thickness.

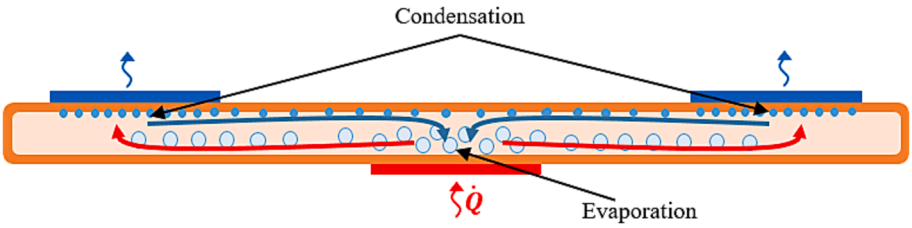

Fig. 3. Performance of the phase-change intermediate heat exchanger.

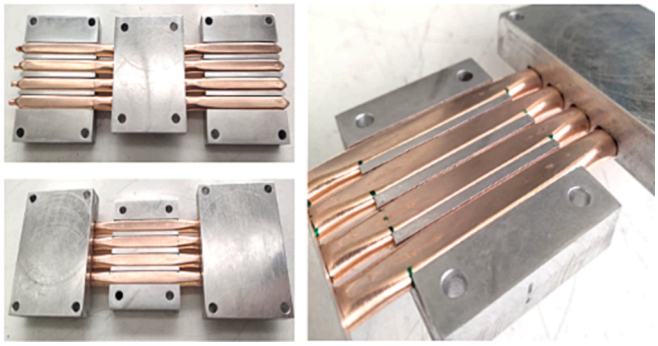

Fig. 4. Developed phase-change intermediate heat exchanger.

Table 1
Resolution and accuracy of the measurement's sensor used.

Sensor	Type	Resolution	Accuracy
Temperature (°C)	NiCr Type K	0.1	±0.5
Voltmeter (V)	ZA9900AB4	0.1	±0.2
Ammeter (A)	ZA9901AB4	0.01	±0.02
Anemometer (m/s)	FVAD 35 TH5	0.01	±0.2—2 % of measured value

The experimental uncertainty of the obtained thermal resistances have been calculated using Eq. (8), where the coefficient 2 corresponds to a confidence interval of the 95 %, b_R is the systematic standard uncertainty and $s_{\overline{R}}$ stands for the random standard uncertainty for the measurement [34].

$$U_R = 2\left(b_R^2 + s_{\overline{R}}^2\right)^{1/2} \tag{8}$$

3.1. Hot and cold side heat exchangers

For the hHX (Fig. 6. a), both, the airflow rate and the dissipated heat flow have an effect on its thermal resistance values. The chosen hHX presents a R_{hHX} between 0.1 and 0.37 K/W depending mostly on the airflow rate, since this heat exchanger is designed to operate in a heat flow range around 100 W. The higher the airflow rate the lower the thermal resistance is. High airflow rate improves the convective coefficient, increasing the heat transmission from the hHX to the airflow. For the experimental tests of the final prototypes, the heated airflow has been selected to be 38 m^3/h, so the hHX thermal resistance is going to be around 0.1 K/W.

Lastly, as it was expected, the thermal resistance of cHX (Fig. 6. b) is constant for the different heat supplies, decreasing its value when the mass airflow increases. For the experimental tests of the final prototype the highest mass airflow has been used for the cHX, presenting a thermal resistance of 0.333 K/W.

3.2. Intermediate heat exchangers characterization

Fig. 7 shows the results of the thermal characterization of the two intHXs when the heat flux transferred is modified from 25 to 150 W. Fig. 7 presents the three replicates, the average value and the uncertainty of the experiments based on equation (8). As it was expected, the monophasic intHX thermal resistance presents a constant value of 0.15 K/W as the heat flux is varied, which validates the previous thermal resistance computational study. In contrast, the thermal resistance of phase-change intHX presents a huge dependence on the amount of transferred heat. The higher the heat flux transferred the lower the resistance value of the phase-change intHX thermal resistance is. The reason for this behaviour is that the higher heat flow through the heat pipes is the better the phase-change heat transfer coefficients are. A reduction on the thermal resistance of the phase-change intHX of the 46 %, from 0.13 K/W to 0.07 K/W, is obtained if the heat flux is increased from 25 to 150 W. It is needed to remark that the thermal resistance of the phase-change intHX is always lower compared to the monophasic intHX one, reaching a 53 % reduction at high heat fluxes.

4. Full prototypes

The aim of this work is to experimentally study the performance of the developed MTEHPs. In fact, it is wanted to analyse and compare the influence of using different intHX onto the *COP* of the systems. Therefore, two prototypes have been built, as it is shown in Fig. 8, where three MTEHPs have been placed in series along the airflow for each technology. As the figure shows several airflow temperature measurement sensors have been placed along the duct, at the inlet and outlet of the first MTEHP and at the outlet of the last MTEHP. Besides, for the first MTEHP, the temperatures of the faces of the TEMs have been measured, as Fig. 1 presents.

The COP value is calculated using Eq. (9), which relates the total heat supplied to the airflow ($\dot{Q}_{h,i}$), and the consumed power by the TEMs ($\dot{W}_{e,i} = \sum \dot{W}_{e,i}^{j}$). The subscript i denotes the number of TEHP located along the airflow, when lacking the subscript i refers to the entire prototype, while the superscript j denotes de stage number.

$$COP_i = \frac{\dot{Q}_{h,i}}{\dot{W}_{e,i}} \tag{9}$$

The heat supply to the airflow is typically achieved by Eq. (10). The total heat supply depends on the temperature difference between outlet ($T_{out,i}$) and inlet ($T_{in,i}$), the heated air mass airflow ($\dot{m}_a = \rho v A$) and its specific heating capacity (c_p).

$$\dot{Q}_{h,i} = (\dot{m}_a c_p)(T_{out,i} - T_{in,i}) \tag{10}$$

In this study, a new methodology to calculate the emitted heat power is proposed. This calculation methodology is based on the energy balance of the thermoelectric system (Fig. 9). Thereby, the dissipated heat from the MTEHP to the airflow is calculated with Eq. (11), which represents the sum of the absorbed heat ($\dot{Q}_{c,i}$), defined by Eq.(12), and the power consumption of all the involved TEMs.

$$\dot{Q}_{h,i} = \dot{Q}_{c,i} + \dot{W}_{e,i} \tag{11}$$

$$\dot{Q}_{c,i} = \sum (T_{amb} - T_{c,i}^{1})/R_{cHX} \tag{12}$$

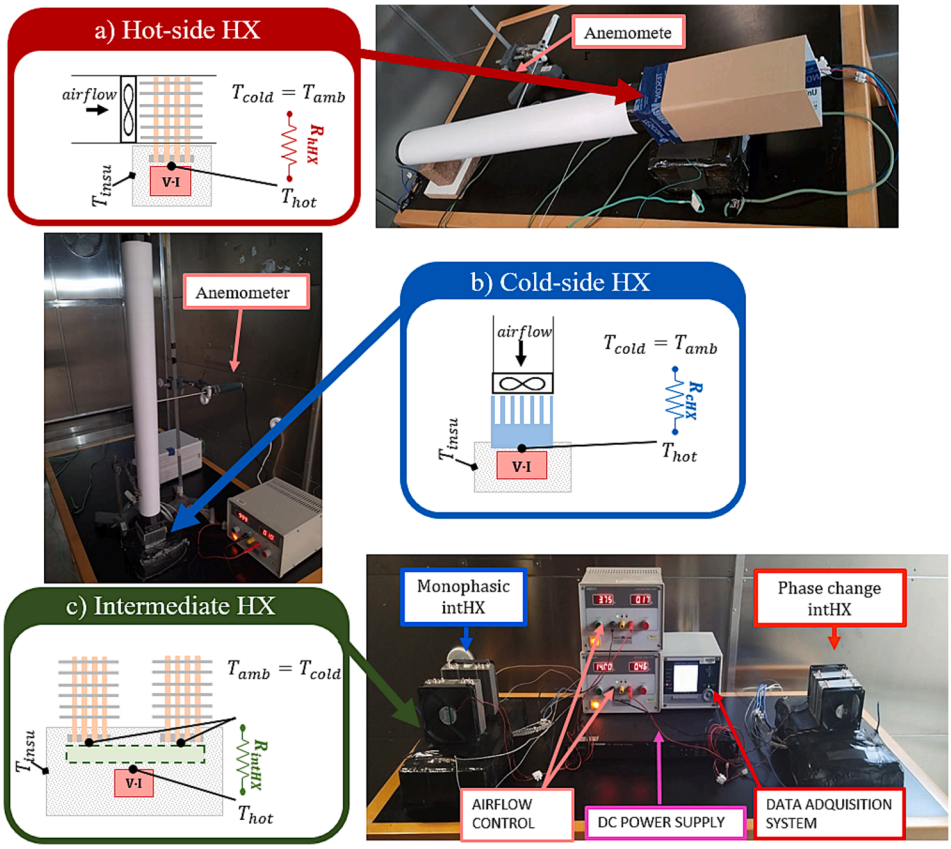

Fig. 5. Heat exchangers thermal characterization test benches: a) hHX; b) cHX and c) intHX.

Table 2
Thermal characterization tests.

Heat Exchanger	Heat flow, $\dot{Q}$ (W)	Airflow Rate (m³/h)
hHX	5, 15, 25, 75, 125, 175	6, 10, 18, 28, 38
cHX	25, 75, 125, 175	18, 26, 34
intHX	25, 50, 75, 100, 125, 150	–

The experimental tests consisted of TEMs voltage supply variation from 2 V to 10 V, connecting all TEMs in parallel configuration for heating an airflow of 38 m^3/h. All tests have been performed in a climate chamber at 26 °C and three replicates where performed to reduce uncertainty. Additionally, a period of minimum 20 min of stationary state was performed per experimental case.

4.1. Validation of the novel methodology to calculate the heat dissipated

Fig. 10 shows the correlation between the two calculation approaches to calculate the $\dot{Q}_{h,1}$ of the first MTEHP based on the experimental data, where the three replicates are shown. The value of the cHX thermal resistance, used in Eq.(12) is the one obtained from the thermal characterization described along section 3 and the consumption of the TEMs has been measured using the voltmeters and ammeters described in Table 1. The outlet temperature of the first MTEHP has been considered as outlet temperature in Eq. (10). The difference in between these two methods is below ± 9 %, which confirms the reliability of this

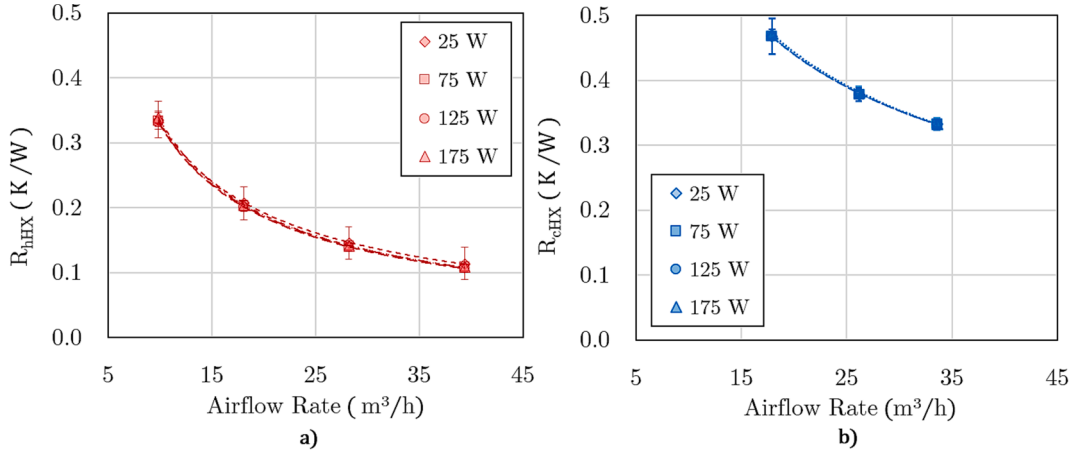

Fig. 6. Thermal resistance characterization of a) hHX and b) cHX.

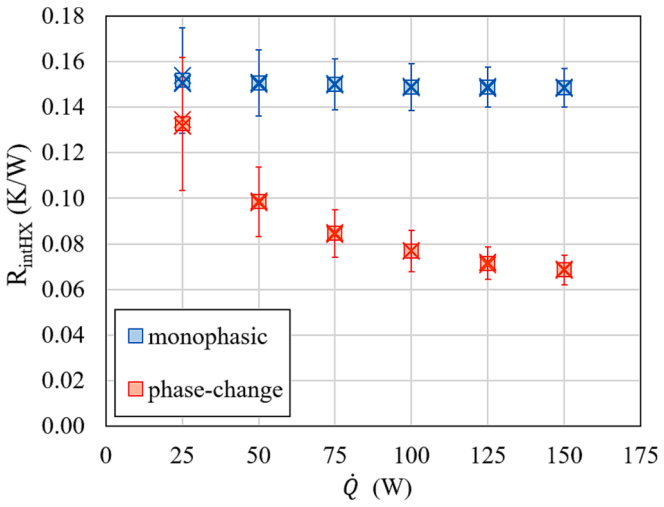

Fig. 7. Thermal characterization of different intermediate heat exchangers.

new methodology to analyse the experimental tests. It could be appreciated how the use of the new methodology to calculate the generated heat for the monophasic prototype slightly overestimates the results. This is attributed to possible heat losses at the intermediate heat exchanger, as the monophasic intHX always presents higher operation temperatures compared to the phase-change one (Table 3).

4.2. Multi-stage TEHP performance

Table 3 shows the total current consumption (I), inlet ($T_{in,1}$), outlet ($T_{out,1}$) temperature, generated heat and coefficient of performance of the first MTEHP, outlet airflow temperature, $\dot{Q}_h$ and COP of the whole system ($T_{out,3}$) when different voltage values (V) are supplied. In addition, the temperatures of all the faces of the TEMs (Fig. 8) of the first MTEHP of each prototype can be encountered. The subscript i denotes the number of TEHP located along the airflow. Meanwhile, the superscript j denotes the stage number. In the case of the second stage temperatures an "a" or a "b" is added, which means its position in the direction of the airflow, being "a" the first one and "b" the second one. The inlet and outlet temperatures of the airflow are defined with the subscript i that denotes de MTEHP. All the measurements have been carried out with the measuring instruments defined in Table 1.

The use of phase-change intHX with a low thermal resistance enables the TEMs to work in a lower temperature difference. Thus, the temperature differences between faces of the TEMs of two-stage thermoelectric system are similar for both stages. Whereas in the one with the monophasic intHX, for high voltage supplies, the TEM of the first stage presents temperature differences much higher than the second stage ones. As a result, the behaviour of the second stage TEMs starts to deteriorate, so the performance of the MTEHP worsens. Moreover, it could be observed that the total COP value is lower than the COP_1 achieved by the first MTEHP of each prototype. This occurs because the airflow temperature raises up by flowing through the duct, hence, the first MTEHP works between lower temperature differences between sources than the subsequent MTEHPs. The temperature difference in between sources is defined by $\Delta T_{sources,i} = T_{air,i} - T_{amb}$, where T_{air} is the mean temperature between the inlet and outlet temperature of the air for each MTEHP, the subscript "i" denotes the number of TEHP located along the airflow and T_{amb} is the constant ambient temperature. The fact of working between higher temperature differences in between the sources increments the natural heat conduction, from the heated airflow to the ambient, because of Fourier effect. Hence, the second and third MTEHPs have to present higher heat absorptions from the ambient (thanks to Pelteir effect) to properly work as heat pumps. If the natural heat conduction is equal to the absorbed heat by Peltier effect, COP values similar to one are obtained, working the thermoelectric heat pumps as electrical resistances. Finally, if the natural heat conduction is greater than the heat absorbed by Pelteir effect, COP values lower than the unit are reached and the MTEHP stops working as a heat pump. Therefore, it is interesting to note the importance of using efficient heat exchangers, as can be seen in the case of a voltage supply of 10 V. The monophasic MTEHP obtains a COP of 0.99, whereas using the phase-change intHX the MTEHP works correctly and reaches a COP of 1.24, a 25 % higher COP than the monophasic prototype.

Fig. 11 shows the heat supplied to the airflow for both prototypes, where the consumed power and the absorbed heat can be consulted for each of the studied different voltage supplies. For all the cases, the obtained $\dot{Q}_h$ by the phase-change MTEHP is higher, achieving a higher outlet airflow temperature ($T_{out,3}$), as Table 3 shows. The novel phase-change MTEHP generated heat is always 16 % higher than the MTEHP with monophasic intHX, obtaining a maximum improvement of the 36

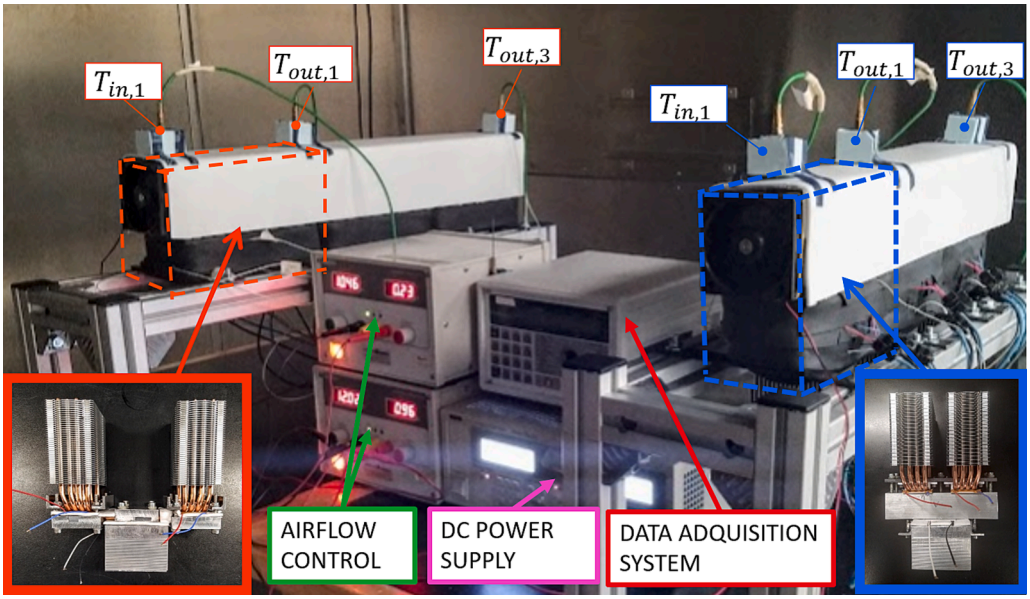

Fig. 8. Test bench for experimental tests of both prototypes in a climate chamber at 26 °C.

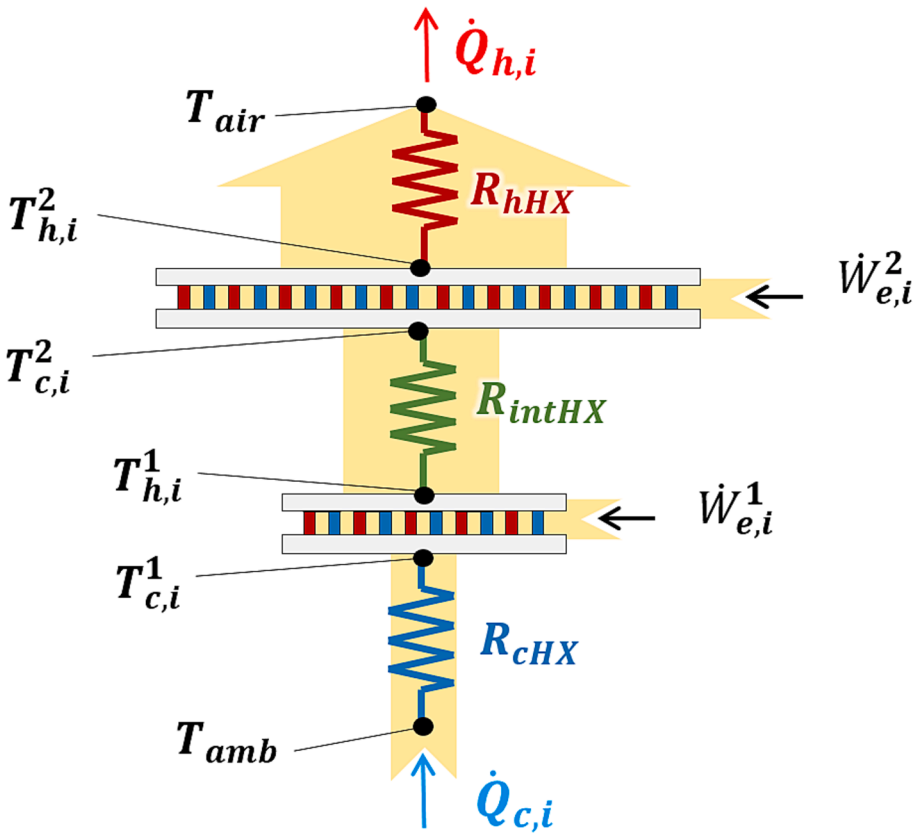

Fig. 9. Heat flow diagram of two-stage thermoelectric heat pump.

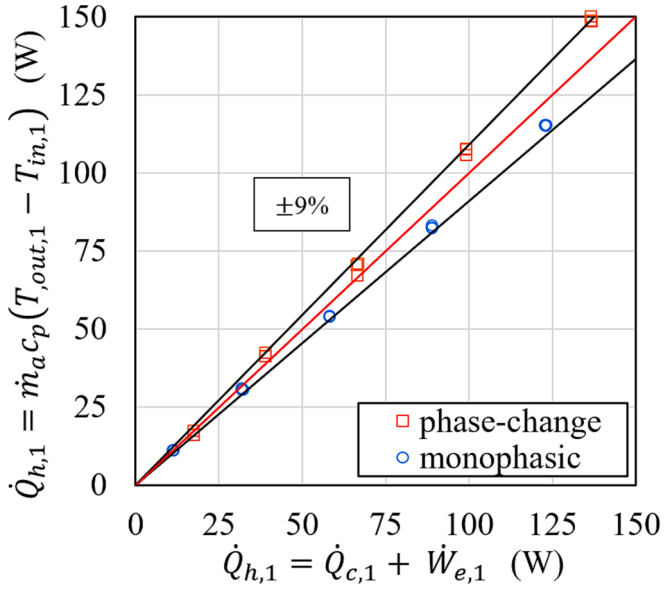

Fig. 10. Validation of generated heat flow by first MTEHP ($\dot{Q}_{h,1}$) for each technology calculated as in Eq. (12) and Eq. (13).

% with a 2 V supply. Moreover, the power consumption of the phase-change MTEHP prototype is always lower than the monophasic one, because it consumes less current for the same voltage supply (Table 3). A minimum reduction of the 6 % is achieved for all the cases, reaching a 13 % reduction at 2 V. Additionally, it can be observed how the monophasic MTEHP cannot perform as a heat pump, as the absorbed heat is negligible, and consequently is behaves as an electrical resistance with a total COP value next to unity.

All the previous facts demonstrate that the development of intHX with small thermal resistances is necessary to obtain efficient MTEHP that could be used to efficiently heat up an airflow, taking into account the inherent benefits of thermoelectric technology.

Fig. 12 presents the COP and the $\dot{Q}_h$ values with their uncertainties calculated by Eq.8 for each type of MTEHP depending on the temperature increase achieved in the airflow. As it was expected, the prototype with phase-change intHX always presents higher *COP* values compared to the ones with monophasic intHX. This occurs due to the low thermal resistance of the phase-change intHX that benefits the operation of the TEHP. As Fig. 12 shows, the temperature lift in the airflow, which is directly related with the temperature difference between reservoirs, determines the *COP* s of the systems. In order to compare both technologies, the same airflow temperature lift range has been taken into account, an airflow heating form 3.5 °C to 23.5 °C. In the case of the phase-change MTEHP the *COP* range is between 1.26 and 3.25, while for the monophasic MTEHP the values are in between 0.99 and 1.95, when the airflow is heated between 23.5 and 3.5 °C, respectively. These figures demonstrate improvements between 30 % and 67 % by using a phase-change intHX instead the conventional monophasic one. The phase-change TEHP is able to heat up the 38 m^3/h airflow 27.7 °C presenting a *COP* of 1.24. To achieve this fact, a heat input of 338.3 W into the airflow is necessary. The use of electric resistances would obtain a COP of 1, consequently, the developed MTEHP is able to outperform the conventional technology a 24 % when the difference in between sources is around 14 °C. Meanwhile, if the difference in between sources decreases to 10 °C an improvement of the 37 % is reached. The obtained COP values show the benefits of using thermoelectric technology to increase the temperature of an airflow, a technology free of refrigerants that can obtain high COPs with very simple, robust, maintenance-free and easily controllable systems.

Table 3
Measured current and temperatures with different voltage supplies for each MTEHP technology.

	V	I	$T_{in,1}$	$T^1_{c,1}$	$T^1_{h,1}$	$T^{2,a}_{c,1}$	$T^{2,a}_{h,1}$	$T^{2,b}_{c,1}$	$T^{2,b}_{h,1}$	$T_{out,1}$	$\dot{Q}_{h,1}$	COP_1	$T_{out,3}$	$\dot{Q}_h$	COP
	(V)	(A)	(°C)	(°C)	(°C)	(°C)	(°C)	(°C)	(°C)	(°C)	(W)	–	(°C)	(W)	–
phase-change MTEHP	2.0	5.67	**25.5**	21.2	22.5	20.9	26.0	20.8	26.8	26.4	16.4	3.76	**28.3**	**40.6**	**3.58**
	4.0	11.45	**25.6**	18.5	22.0	19.5	27.6	19.4	29.4	28.0	41.5	2.36	**32.7**	**95.8**	**2.09**
	6.0	17.09	**25.7**	16.6	23.8	20.4	29.5	20.3	32.5	30.6	69.4	1.76	**38.5**	**162.8**	**1.59**
	8.0	22.45	**25.8**	15.8	27.6	23.4	32.0	23.4	36.5	33.9	107.0	1.55	**45.6**	**246.3**	**1.37**
	10.0	27.39	**26.0**	15.6	33.5	28.4	35.0	28.4	41.0	37.8	149.0	1.41	**53.7**	**338.3**	**1.24**
monophasic MTEHP	2.0	6.51	**25.6**	23.3	25.0	23.6	27.5	23.5	28.1	26.43	11.2	2.40	**27.3**	**29.8**	**2.29**
	4.0	12.83	**25.6**	21.0	26.0	23.3	28.7	23.0	30.1	28.01	30.6	1.67	**31.3**	**78.7**	**1.53**
	6.0	18.78	**25.7**	19.7	29.4	25.3	30.2	25.0	32.6	30.02	54.1	1.34	**36.3**	**140.8**	**1.25**
	8.0	24.21	**26.0**	19.2	34.9	29.4	32.2	29.1	35.6	32.50	82.5	1.19	**42.1**	**211.3**	**1.09**
	10.0	29.08	**26.3**	19.7	42.4	35.5	34.4	35.4	39.2	35.44	115.1	1.11	**49.0**	**289.3**	**0.99**

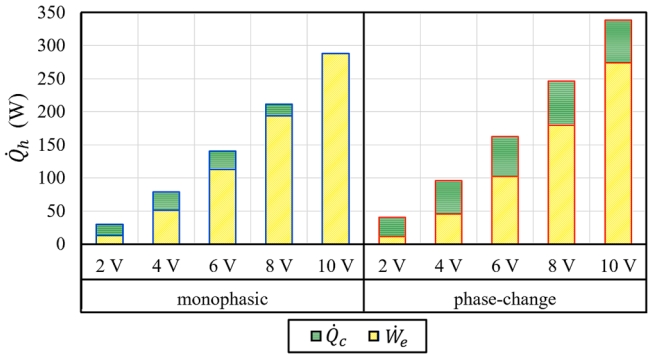

Fig. 11. $\dot{Q}_h$, which is the sum of $\dot{Q}_c$ and $\dot{W}_e$ (Eq. (11), of the two types of MTEHP prototypes for different voltage supply.

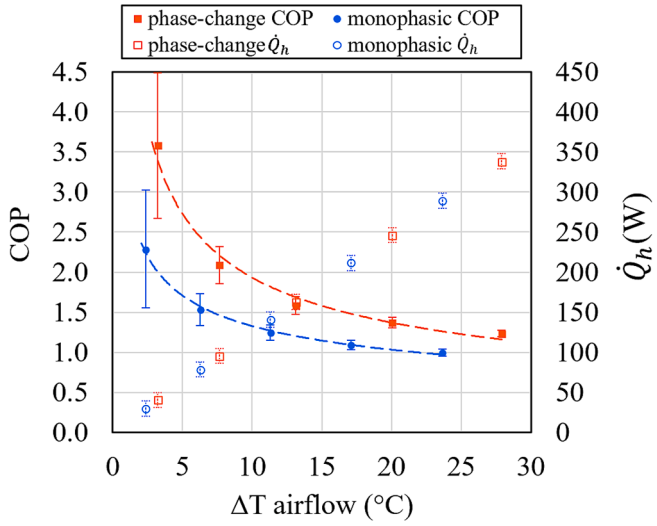

Fig. 12. COP and generated heat $\dot{Q}_h$ of the two types of MTEHP prototypes.

5. Conclusion

The need to make an energy transition toward renewable energies has deliberated on the necessity of electrifying the energy system. One of the most promising sectors to electrify is heating and cooling sector, which end use energy supposes a half of the total consumed energy in the world. Therefore, it is necessary to develop new equipment capable of efficiently supplying heating needs, environmentally friendly and with a long-life cycle.

In this manuscript the use of thermoelectric technology working as a heat pump for heating up an airflow is presented. Two different multistage thermoelectric heat pumps have been designed, built and tested. The difference between them is the heat transfer phenomena used for the intermediate heat exchanger, the one in between stages, building a conventional monophasic intHX based on an optimized aluminium block and a novel phase-change intHX that efficiently transfers the heat from the first to the second stage. Both MTEHP prototypes have been built and experimentally tested under the same operational conditions of 26 °C ambient temperature to heat an airflow rate of 38 m^3/h. The phase-change intHX prototype reaches COPs of 1.26——3.25 for airflow temperature increments between 23.5 and 3.5 °C, improving the COP values between a 30 % and a 67 % with respect to the monophasic prototype. This is because the phase-change MTEHP supplied more heat to the airflow by consuming a less of power thanks to the innovative phase-change intermediate heat exchanger presented along this manuscript.

Moreover, this experimental study has proven a novel methodology to calculate the generated heat by MTEHP. This methodology is based on the energy balance of the thermoelectric system. The heat rejected is calculated as the sum of the heat absorbed from the cold side and the power consumption of the TEMs. This new methodology has been validated and a discrepancy of the ± 9 % between the novel methodology and the conventional one based on the airflow temperature rise can be found.

As an overall conclusion, this work presents an experimental study of the potential application of thermoelectric heat pumps for heating up an airflow thanks to the design and development of a novel phase-change intermediate heat exchanger that enables a very efficient thermoelectric multistage configuration.

Declaration of competing interest

The authors declare that they have no known competing financial interests or personal relationships that could have appeared to influence the work reported in this paper.

Data availability

The authors do not have permission to share data.

Acknowledgment

The authors would like to acknowledge the support of the Government of Navarre, as part of the “Grants to SINAI agents for the realization of collaborative R&D projects” under the PC066-067-068 FlexORCStorage projects and PC116-117-118 MASS-STORAGE projects. Open access funding provided by Universidad Pública de Navarra.

References

[1] F. Boshell, D. Russo, B. Hong Loan Officer, G. Prakash, E. Asmelash, L. Janeiro, J. Liu, J. Feng, N. Zhang, X. Liu, L. Liu, S. Li, F. Tang, C. Zhang, J. Li, L. Xing, P. Komor, N. Wagner, Y. Li, A. Scheer of IRENA, L. Jiang, Y. Wang, G. Lu, B. Shan, H. Dai, H. Zheng of SGERI, SMART ELECTRIFICATION WITH RENEWABLES Driving the transformation of energy services Citation, 2022.

[2] Z. Guzović, N. Duić, A. Piacentino, N. Markovska, B.V. Mathiesen, H. Lund, Paving the way for the Paris Agreement: Contributions of SDEWES science, Energy. 263 (2023), https://doi.org/10.1016/j.energy.2022.125617.
[3] European Commission, 2050 long-term strategy | Climate Action, n.d.
[4] T. Goodson, F. Briens, C. Camarasa, C. Delmastro, L. Staas, K. Petrichenko, IEA (2022), Heating, IEA, Paris https://www.iea.org/reports/heating, 2022. https://www.iea.org/reports/heating.
[5] H. Ümitcan Yilmaz, R. Hartel, D. Keles, R. Mckenna, W. Fichtner, M. Mikulić, D. Balić, D. Jakšić, A. Chiodi, R. de Miglio, Analysis of the potential for Power-to-Heat/Cool applications to increase flexibility in the European electricity system until 2030 About INSIGHT_E, 2017. www.insightenergy.org.
[6] A. Bloess, W.P. Schill, A. Zerrahn, Power-to-heat for renewable energy integration: A review of technologies, modeling approaches, and flexibility potentials, Appl Energy. 212 (2018) 1611–1626, https://doi.org/10.1016/j.apenergy.2017.12.073.
[7] P.C. Slorach, L. Stamford, Net zero in the heating sector: Technological options and environmental sustainability from now to 2050, Energy Convers Manag. 230 (2021), 113838, https://doi.org/10.1016/j.enconman.2021.113838.
[8] U. Roobab, A.W. Khan, M. Irfan, G.M. Madni, X.A. Zeng, A. Nawaz, N. Walayat, M. F. Manzoor, R.M. Aadil, Recent developments in ohmic technology for clean label fruit and vegetable processing: An overview, J Food Process Eng. 45 (2022), https://doi.org/10.1111/jfpe.14045.
[9] C. Yue, Y. Zhang, W. Lu, Y. Zhang, P. Wang, Y. Li, H. Zhou, Realizing the curing of polymer composite materials by using electrical resistance heating: A review, Compos Part A Appl Sci Manuf. 163 (2022), https://doi.org/10.1016/j.compositesa.2022.107181.
[10] T. Abergel, Heat Pumps – Analysis - IEA (2021).
[11] D. Rowe, B. Raton London New York, Thermoelectrics Handbook, CRC Press, 2018. 10.1201/9781420038903.
[12] C. Wang, L. Hua, H. Yan, B. Li, Y. Tu, R. Wang, A Thermal Management Strategy for Electronic Devices Based on Moisture Sorption-Desorption Processes, Joule. 4 (2020) 435–447, https://doi.org/10.1016/j.joule.2019.12.005.
[13] A. Çağlar, Design and experimental investigation of a novel thermoelectric water dispenser unit, Appl Therm Eng. 149 (2019) 822–828, https://doi.org/10.1016/j.applthermaleng.2018.11.028.
[14] K.R. Gluesenkamp, P. Boudreaux, V.K. Patel, D. Goodman, B. Shen, An efficient correlation for heat and mass transfer effectiveness in tumble-type clothes dryer drums, Energy. 172 (2019) 1225–1242, https://doi.org/10.1016/j.energy.2019.01.146.
[15] W. He, P. Yu, Z. Hu, S. Lv, M. Qin, C. Yu, Experimental study and performance analysis of a portable atmospheric water generator, Energies (basel). 13 (2019), https://doi.org/10.3390/en13010073.
[16] H. Lim, Y.K. Kang, J.W. Jeong, Thermoelectric radiant cooling panel design: Numerical simulation and experimental validation, Appl Therm Eng. 144 (2018) 248–261, https://doi.org/10.1016/j.applthermaleng.2018.08.065.
[17] Y.W. Kim, J. Ramousse, G. Fraisse, P. Dalicieux, P. Baranek, Optimal sizing of a thermoelectric heat pump (THP) for heating energy-efficient buildings, Energy Build. 70 (2014) 106–116, https://doi.org/10.1016/j.enbuild.2013.11.021.
[18] S. Diaz de Garayo, A. Martínez, D. Astrain, Optimal combination of an air-to-air thermoelectric heat pump with a heat recovery system to HVAC a passive house dwelling, Appl Energy. 309 (2022), https://doi.org/10.1016/j.apenergy.2021.118443.
[19] B. Hou, Y. Zheng, L. Xing, Q. Song, Performance of a thermoelectric heat pump with recirculation and regenerative heat recovery, Appl Therm Eng. 223 (2023), https://doi.org/10.1016/j.applthermaleng.2023.120042.
[20] S. Diaz de Garayo, A. Martínez, P. Aranguren, D. Astrain, Prototype of an air to air thermoelectric heat pump integrated with a double flux mechanical ventilation system for passive houses, Appl Therm Eng. 190 (2021), 116801, https://doi.org/10.1016/j.applthermaleng.2021.116801.
[21] X.D. Wang, Q.H. Wang, J.L. Xu, Performance analysis of two-stage TECs (thermoelectric coolers) using a three-dimensional heat-electricity coupled model, Energy. 65 (2014) 419–429, https://doi.org/10.1016/j.energy.2013.10.047.
[22] H. Sun, S.U. Gil, W. Liu, Z. Liu, Structure optimization and exergy analysis of a two-stage TEC with two different connections, Energy. 180 (2019) 175–191, https://doi.org/10.1016/j.energy.2019.05.077.
[23] J. Chen, J. Yu, M. Ma, Theoretical study on an integrated two-stage cascaded thermoelectric module operating with dual power sources, Energy Convers Manag. 98 (2015) 28–33, https://doi.org/10.1016/j.enconman.2015.03.090.
[24] Y.H. Cheng, C. Shih, Maximizing the cooling capacity and COP of two-stage thermoelectric coolers through genetic algorithm, Appl Therm Eng. 26 (2006) 937–947, https://doi.org/10.1016/j.applthermaleng.2005.09.016.
[25] L. Chen, J. Li, F. Sun, C. Wu, Performance optimization for a two-stage thermoelectric heat-pump with internal and external irreversibilities, Appl Energy. 85 (2008) 641–649, https://doi.org/10.1016/J.APENERGY.2007.10.005.
[26] H. Nami, A. Nemati, M. Yari, F. Ranjbar, A comprehensive thermodynamic and exergoeconomic comparison between single- and two-stage thermoelectric cooler and heater, Appl Therm Eng. 124 (2017) 756–766, https://doi.org/10.1016/j.applthermaleng.2017.06.100.
[27] L.G. Chen, F.K. Meng, Y.L. Ge, H.J. Feng, S.J. Xia, Performance optimization of a class of combined thermoelectric heating devices, Sci China Technol Sci. 63 (2020) 2640–2648, https://doi.org/10.1007/s11431-019-1518-x.
[28] R. Arora, R. Arora, Multiobjective optimization and analytical comparison of single- and 2-stage (series/parallel) thermoelectric heat pumps, Int J Energy Res. 42 (2018) 1760–1778, https://doi.org/10.1002/er.3988.
[29] RC12-6-01LS Marlow Industries, Inc. | Fans, Thermal Management | DigiKey, (n.d.). https://www.digikey.es/en/products/detail/marlow-industries-inc/RC12-6-01LS/6159103?s=N4IgTCBcDaIEoGECMYC0A2VAGJAZAyiALoC%2BQA (accessed January 28, 2022).
[30] D. Astrain, J.G. Vián, M. Domínguez, Increase of COP in the thermoelectric refrigeration by the optimization of heat dissipation, Appl Therm Eng. 23 (2003) 2183–2200, https://doi.org/10.1016/S1359-4311(03)00202-3.
[31] S. Lee, S. Song, V. Au, K.P. Moran, Constriction/Spreading Resistance Model for Electronics Packaging, 4th ASME/JSME Thermal Eng, Joint Conf. 4 (1995) 199–206.
[32] Advanced Thermal Solutions Inc., Round Heat Pipe ATS-HP5D8L200S77W-148 DataSheet., (n.d.). https://www.digikey.com/es/products/detail/advanced-thermal-solutions-inc/ATS-HP-D8L200S77W-148/7899889.
[33] P. Aranguren, S. DiazDeGarayo, A. Martínez, M. Araiz, D. Astrain, Heat pipes thermal performance for a reversible thermoelectric cooler-heat pump for a nZEB, Energy Build. 187 (2019) 163–172, https://doi.org/10.1016/j.enbuild.2019.01.039.
[34] H.W. Coleman, W.G. Steele, Experimentation, validation, and uncertainty analysis for engineers, 3rd ed.,, 2019.